stellarator news

Published by Fusion Energy Division, Oak Ridge National Laboratory
Building 9201-2 P.O. Box 2009 Oak Ridge, TN 37831-8071, USA

Editor: James A. Rome Issue 49 January 1997
E-Mail: jar@ornl.gov Phone: (423) 574-1306 Fax: (423) 241-6211
On the Web at *http://www.ornl.gov/fed/stelnews*

Anniversary issue

This issue marks the start of the ninth year of bimonthly publication for Stellarator News. The Editor wishes to thank Bonnie Nestor (ORNL) for her outstanding editorial assistance.

The articles in this issue show that the stellarator community is an exciting venue for fusion research. New machines are coming online, a modern reactor study has been completed, and even better new configurations are being proposed. Finally, two mature devices report the very important effects of heating methods on the radial potential which may have profound effects on transport.

TJ-II flux surfaces

In the last issue of *Stellarator News*, we reported that the final assembly of the Spanish heliac TJ-II (CIEMAT, Madrid) was complete. In mid-December, the Spanish team succeeded in measuring the TJ-II flux surfaces (see Fig. 1), thus verifying the gross accuracy of the complicated magnetic coil configuration.

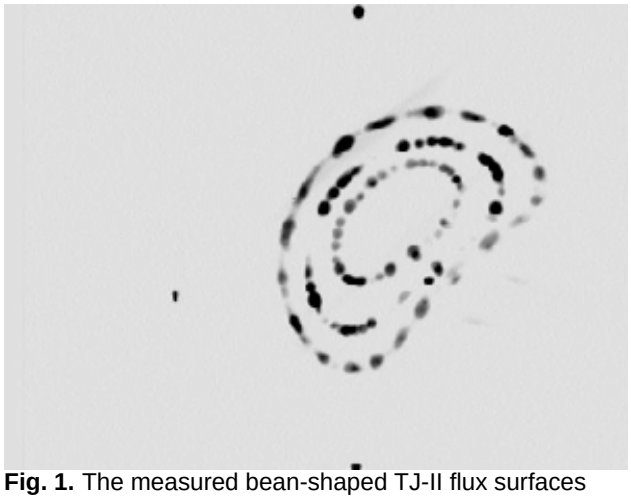

Fig. 1. The measured bean-shaped TJ-II flux surfaces are shown with three fixed reference lights.

In this issue . . .

U.S. Stellarator Power Plant Study (SPPS)

Work has been completed on the Stellarator Power Plant Study (SPPS) [see *Stellarator News*, Issue #32 (March 1994), p. 7]. Participants in the study included a broad representation of the stellarator physics community, as well as a subset of the multi-institutional ARIES Team, augmented by specialized industrial support.

Generally, conceptual power plant design studies extrapolate from the present knowledge base to characterize the future economic and environmental features of competing approaches. The SPPS addresses a widely perceived need to consider non-tokamak alternative power plant options in the post-ITER period. Limited in scope and depth relative to the ARIES tokamak-based studies, the SPPS focused on the consensus identification of a reference configuration, the modular, Helias-like Heliac (MHH), and applied engineering assumptions, constraints, and extrapolations consistent with the ARIES tokamak studies to address key issues for the stellarator approach.

The SPPS/MHH projects a 1,000-MWe (net), DT-fueled central power station, with key parameters summarized in Table 1. The baseline MHH configuration has four field periods, produced by 32 modular, nonplanar coils of four distinct types.

Table 1: SPPS/MHH Parameter Summary

Plasma major toroidal radius, R_T (m)	13.95
Plasma aspect ratio, $A = R_T/r_p$	8.5
Circularized (average) plasma radius, r_p (m)	1.63
Plasma volume, V_p (m^3)	734.7
Plasma beta	0.05
Lackner-Gottardi confinement multiplier, H	2 .3
On-axis toroidal field, B_0 (T)	4.94
Field at TF coil (maximum), B_c (T)	14.5
Fusion power, P_F (GW)	1.73
Thermal conversion efficiency	0.46
Thermal power, P_{TH} (GWth)	2.29
Gross electrical power, P_{ET} (GWe)	1.05
Net electrical power, P_E (GWe)	1
Recirculating power fraction	0.05
Total direct cost ($\$ \times 10^6$)[a]	2,249
Plant capacity factor, p_f	0.76
Total capital cost ($\$ \times 10^6$)[b]	4,340
Cost of electricity, COE (mill/kWeh)	74.6

[(a)] assumes 10th-of-a-kind learning-curve credits and certain safety-related cost credits.
[(b)] assumes 6-year construction lead time.

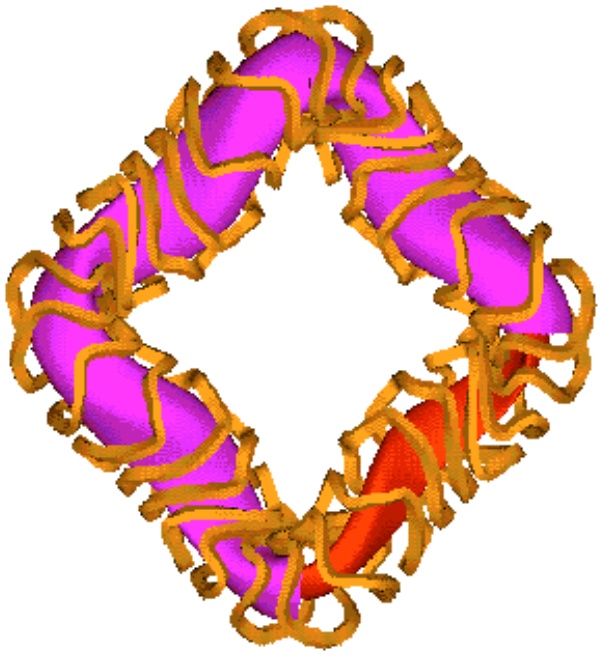

Fig. 1. A top view of the MHH coil configuration, with the blanket/shield between the plasma and the coils.

Compared to a tokamak reactor, the recirculating power is low because of the absence of a current drive requirement. System power density is typically lower because of the requirement for a minimum plasma-coil spacing at higher plasma aspect ratio. The engineering configuration is complicated by the helical plasma geometry, but fundamental choices of materials and coolants are shared with the tokamak approach. A critical design constraint is the desire to minimize the distance between the inboard plasma edge and the coil winding pack consistent with adequate tritium breeding in the lithium-bearing blanket and sufficient neutronic shielding of the coils. The reference blanket/coolant configuration invokes a vanadium-alloy structure (with CaO-coated coolant channels to reduce MHD pumping power) with low-activation properties that is cooled by flowing liquid lithium.

Physics issues for the MHH include equilibrium/stability at the reference beta value of 5%, the influence of magnetic islands on divertor geometry, neoclassical transport in the presence of electric fields, suppression of the bootstrap current, and startup/control scenarios. MHH physics performance is projected to be adequate and robust.

Engineering emphasis is on the coil design, neutronics optimization, integration of the blanket/shield/divertor systems into the MHH configuration, and assessment of a suitable maintenance approach. A suitable divertor/blanket/shield configuration can be accommodated in MHH-based fusion power plants and maintained. A preliminary, but detailed, assessment of Nb_3Sn cable-in-conduit conductor (CICC) graded, modular,

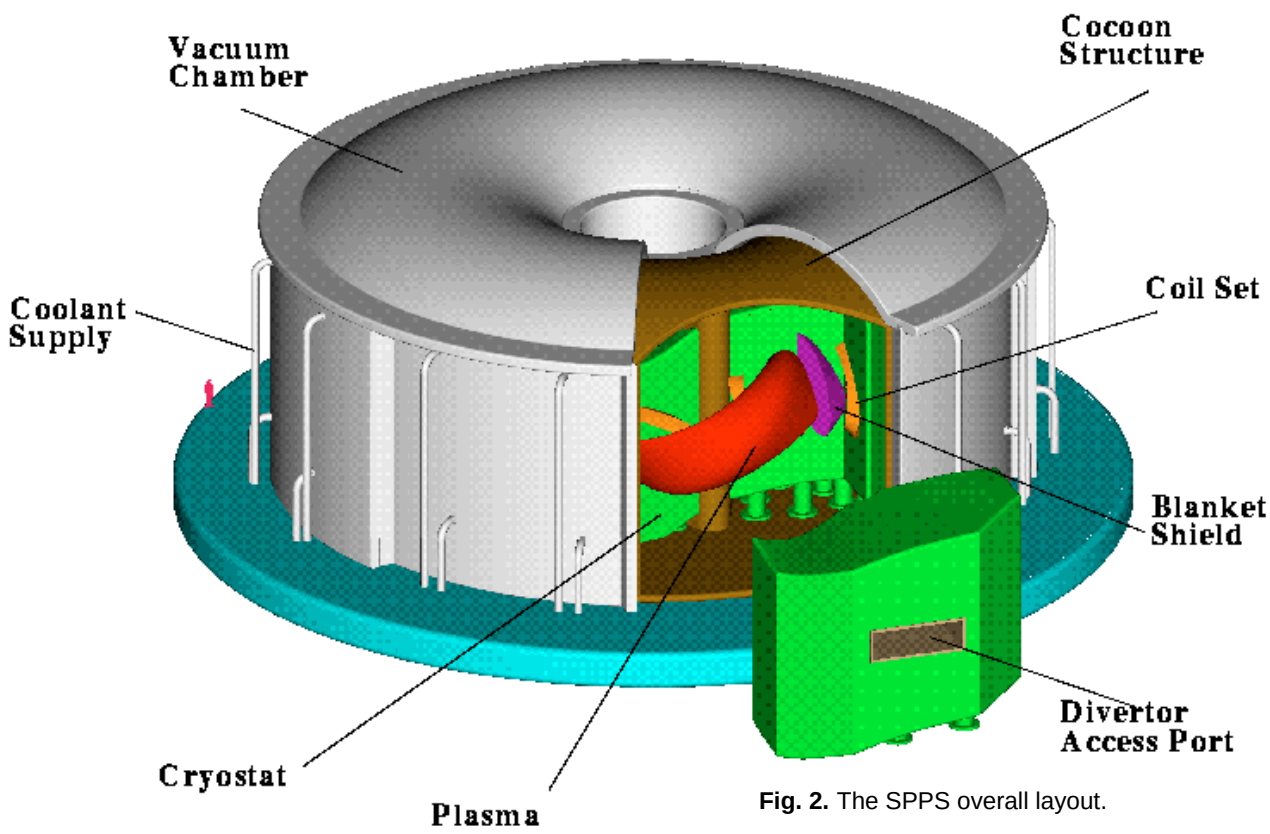

Fig. 2. The SPPS overall layout.

nonplanar coils at 14.5 T is encouraging. The MHH as examined in the SPPS was found to be cost competitive with tokamak approaches. Further reductions in the over - all size of the fusion power core, with corresponding increases in the system power density, may be required to improve competitiveness.

A top view of the MHH coil configuration, with the blanket/shield enclosing the plasma, is illustrated in Fig. 1.

The SPPS/MHH fusion power core is illustrated sche - matically in Fig. 2. Access for maintenance is provided through four large ports at the corners of the MHH con - figuration. Sets of modular coils and the underlying blanket/shield assemblies would be clustered into mov - able units for transport to the hot cell.

The MHH configuration, selected for emphasis in the SPPS, is one of a number of credible stellarator embodi - ments. Other interesting variations of the MHH configu - ration were not explored in detail.

The SPPS effort is documented in Ref. [1]. Evolving summary information regarding the SPPS and other power plant studies performed by the ARIES Team can be found on the World Wide Web at the URL:
http://aries.ucsd.edu/PUBLIC/RESEARCH/ARIES/ARIES.html

Ronald L. Miller
University of California, San Diego
Fusion Energy Research Program, Engineering Building, Unit II
9500 Gilman Drive, Mail Code 0417, La Jolla, CA 92093-0417
Phone: (619) 534-7842
Fax: (619) 534-7716 460
Email: miller@fusion.ucsd.edu

Reference

[1] R. L. Miller (Ed.) and the SPPS Team, *The Stellarator Power Plant Study*, UCSD-ENG-004, University of California, San Diego (to be published 1996).

Average drift velocity of trapped particles in stellarators

The normal to a magnetic surface component of the bounce-averaged velocity of trapped-particle drift is of special interest. We denote this component by v_{an}. It is known from neoclassical transport theory (see, e.g., [1]) that when the effective collision frequency for trapped particles is less than the trapped-particle bounce frequency, the difference of v_{an} from zero leads in stellarators to a significant increase of coefficients of the transport across magnetic surfaces in comparison with the case of an axially or helically symmetric magnetic field, where $v_{an} = 0$. For example, the $1/\nu$ transport regime is characteristic for standard stellarators due to the above effect.

Qualitatively, for rather small collision frequencies the neoclassical transport coefficients in stellarators are proportional to the square of v_{an}. So, v_{an} is an interesting parameter which allows one to estimate the relative neoclassical transport in stellarator magnetic configurations.

For specific stellarator magnetic configurations, numerical methods must be used for the evaluation of the neoclassical properties. The necessary computations are frequently performed in magnetic coordinates (see, e.g., Ref. [2]). To compute the magnetic coordinates for a given stellarator magnetic field in Cartesian coordinates is a rather complicated task. Here we consider a method of performing a direct numerical calculation of v_{an} in stellarators with a given magnetic field without using magnetic coordinates.

We assume that the magnetic field $\vec{B}$ of the system under consideration is purely a vacuum field and the electric field $\vec{E}$ is a potential field $\left(\vec{E} = -\nabla\varphi\right)$ with the potential φ assumed to be a function of the magnetic surfaces alone. In this case we can write the drift equations for a charged particle motion in the form [3,4]

$$\frac{d\vec{r}}{dt} = v_{\parallel}\frac{\vec{B}}{B} + \vec{v}_d, \qquad (1)$$

$$\frac{dv_{\parallel}}{dt} = -\frac{1}{2}J_{\perp}\left(\vec{B}\cdot\nabla B\right)/B, \qquad (2)$$

$$\vec{v}_d = \frac{mc}{2eB^3}\left(2v_{\parallel}^2 + J_{\perp}B\right)\left[\vec{B}\times\nabla B\right] + \frac{c}{B^2}\left[\vec{E}\times\vec{B}\right], \qquad (3)$$

where $J_{\perp} = v_{\perp}^2/B$ is the transverse adiabatic invariant.

We also suppose (as it common in neoclassical transport theory) that the Larmor radius of a particle and the electric field are rather small, and consequently the displacement of the particle across a magnetic field line during one bounce period is insignificant. Therefore it is possible to neglect as a first approximation the second term in the right-hand side of Eq. (1) and to solve Eqs. (1) and (2) by the method of integration along a magnetic field line. Equation (3) is used in this case for calculating the particle drift velocity across a magnetic field line.

We are interested in the $\vec{v}_d$ component which is normal to a magnetic surface

$$v_{dn} = \vec{n}\cdot\vec{v}_d, \qquad \vec{n} = \nabla\Psi/|\nabla\Psi|,$$

where $\vec{n}$ is a unit vector of the normal to a magnetic surface, and Ψ is the magnetic surface function ($\vec{B}\cdot\nabla\Psi = 0$). For the $\nabla\Psi$ calculation we use the method of Ref. [5].

As a result, we arrive at the following system of equations:

$$\frac{d\vec{r}}{dt} = v_{\parallel}\frac{\vec{B}}{B}, \qquad (4)$$

$$\frac{dv_{\parallel}}{dt} = -\frac{1}{2}J_{\perp}\left(\vec{B}\cdot\nabla B\right)/B, \qquad (5)$$

$$\frac{dP}{dt} = -\frac{v_{\parallel}}{B}\left(\frac{\partial B^1}{\partial\xi_1}P + \frac{\partial B^2}{\partial\xi_1}Q + \frac{\partial B^3}{\partial\xi_1}G\right), \qquad (6)$$

$$\frac{dQ}{dt} = -\frac{v_{\parallel}}{B}\left(\frac{\partial B^1}{\partial\xi_2}P + \frac{\partial B^2}{\partial\xi_2}Q + \frac{\partial B^3}{\partial\xi_2}G\right), \qquad (7)$$

$$\frac{dG}{dt} = -\frac{v_{\parallel}}{B}\left(\frac{\partial B^1}{\partial\xi_3}P + \frac{\partial B^2}{\partial\xi_3}Q + \frac{\partial B^3}{\partial\xi_3}G\right), \qquad (8)$$

$$\frac{dr_n}{dt} = v_{dn}. \qquad (9)$$

In Eqs. (6)–(8), B^1, B^2 and B^3 are contravariant components of the vector $\vec{B}$ (in a normal curvilinear system of coordinates (ξ_1, ξ_2, ξ_3), and $\partial\Psi/\partial\zeta_1$, $\partial\Psi/\partial\zeta_2$, and $\partial\Psi/\partial\zeta_3$ are represented through P, Q, and G. The multiplier $v_{\parallel}/B$ on the right-hand sides of these equations corresponds to the variable of integration t.

Calculating $\vec{r}$, $v_{\parallel}$, and $\nabla\Psi$ with the help of the system of equations (4)–(7) and simultaneously solving Eq. (9), the right-hand side of which is determined by Eq. (3) and the definition of v_{an}, we shall find for each moment of time t a value of the trapped-particle displacement r_n across a magnetic surface. After dividing the displacement δr_n obtained during a bounce period by the duration of this period τ_b, we obtain an average drift velocity for a trapped-particle guiding center across a magnetic surface, $v_{an} = \delta r_n/\tau_b$.

To calculate v_{an} in a specific stellarator magnetic configuration it is convenient to use the following method. For the magnetic surface of interest let us take the surface part which corresponds to one magnetic field period. Within this part we select some magnetic field lines for which we wish to calculate v_{an}. For each of these lines, the point corresponding to a minimum B value is taken as the initial point of integration in Eqs. (4)–(9). The initial values of $\nabla\Psi$ at these points are determined using the method of Ref. [5] concurrently with the magnetic surface computation. Solving Eqs. (4)–(9) under such initial conditions, one can obtain the

v_{an} distribution as a function of the initial value of the particle longitudinal velocity $v_{\|i}$ and the position of the considered segment of the magnetic field line on the magnetic surface. It is convenient to present the calculation results in a normalized form as the dependence of η on γ, where the parameters η and γ are related to the quantities v_{an} and $v_{\|i}$ by

$$\eta = v_{an}\frac{R}{v_{\perp 0} r_{L0}}, \quad \gamma = v_{\|i}/v_{\perp 0}. \tag{10}$$

Here $v_{\perp 0} = (J_\perp B_0)^{1/2}$, B_0 is the average value of the longitudinal magnetic field, $r_{L0} = mcv_{\perp 0}/eB_0$ is the Larmor radius, calculated for $B = B_0$, and R is the major radius of the torus. Use of the relation for η and v_{an} allows us to perform a convenient comparison of the drift velocity v_{an} in various magnetic configurations. In particular, for the frequently used model of a standard stellarator magnetic field with a circular magnetic surface cross section, the amplitude of the η distribution over a magnetic surface equals (see, e.g., Ref. [1])

$$\eta_m = 0.5 .$$

As an example of the use of this method, we present the results of the calculations of v_{an} for a model magnetic field which is appropriate for a zero-beta variant of the toroidal quasihelically symmetric stellarator [6]. The magnetic field was approximated by a superposition of toroidal harmonic functions containing the associated Legendre functions. The number of the decomposition terms used was limited by the conditions $0 \le n \le 12$, $m = m_p M$, $|M| \le 12$, where n and m are the poloidal and toroidal harmonic numbers, m_p is the number of periods along the torus ($m_p = 6$). The decomposition coefficients of the superposition were found by minimizing the magnetic field component that is normal to the given boundary magnetic surface [6].

The results obtained for the near-boundary magnetic surface are as follows. For this surface, the $\gamma \approx 0.5$ value corresponds to the transition from particles trapped within one magnetic field period to particles that are untrapped or trapped within two or more periods. For all magnetic field lines it appears that $\eta \ll 1$ for rather small γ; i.e., for deeply trapped particles v_{an} is practically equal to zero. But for particles with a mean depth of trapping and $\gamma < 0.5$, v_{an} is not equal to zero. Its distribution over the magnetic surface is periodic with the amplitude depending on γ. For these particles the η amplitude, η_m, reaches the maximum value for $0.3 \le \gamma < 0.5$ and is in the range $\eta_m = 0.25$ to $\eta_m = 0.3$. For particles corresponding to $\gamma \ge 0.5$, v_{an} appears to be small. So, for particles with a mean trapping depth and rather close to the transition between untrapped and trapped within two or more magnetic field periods, v_{an} differs from zero, though it is approximately equal to only half of the velocity obtained analytically for a standard stellarator model [1]. Therefore, we expect an approximately four-fold reduction of the coefficients of neoclassical transport in the magnetic field considered compared to the corresponding coefficients obtained theoretically for the standard stellarator model for equivalent sizes.

The method proposed has allowed us to investigate the average velocity of the trapped-particle drift in complex magnetic fields across any magnetic surface. This can be used for the analysis of plasma confinement in real stellarator magnetic configurations. Minimization of the η parameter is one of the ways of optimizing stellarator systems.

V. V. Nemov
Institute of Plasma Physics, National Science Center
Khar'kov Institute of Physics and Technology
Khar'kov 310108, Ukraine

References

[1] A. A. Galeev and R. Z. Sagdeev, in Voprosy Teorii Plazmy (Problems of Plasma Theory), Atomizdat, Moscow, No. 7, 205 (1973).

[2] A. H. Boozer and G. Kuo-Petravic, Phys. Fluids **24**, 851 (1981).

[3] D. V. Sivukhin in Voprosy Teorii Plazmy (Problems of Plasma Theory), Gosatomizdat, Moscow, No. 1, 7 (1963).

[4] A. I. Morozov and L. S. Solov'ev, ibid, No. 2, 177 (1963).

[5] V. V. Nemov, Nucl. Fusion **28**, 1727 (1988).

[6] J. Nührenberg and R. Zille, Phys. Lett. A **129**, 113 (1988).

Shear-related confinement and the electron root in W7-AS

W7-AS with its almost shearless vacuum configuration was operated in a hybrid mode with significant plasma currents. Stationary profiles of the rotational transform with positive or negative magnetic shear were introduced by inductive and/or electron cyclotron (EC)-driven currents in the direction co and counter to the confining magnetic field. Confinement was investigated in both net-current-free and current-carrying discharges.

The confining magnetic field in the W7-AS stellarator has a "built-in" flat profile of the rotational transform, ι. The magnetic shear is weakly positive (ι'/ι up to +2%) above $\iota = 0.4$ and weakly negative below (up to −2%). Low-order rational values of ι can thus be excluded from the confinement region by a proper choice of ι, which can be varied over a wide range, $0.25 < \iota < 0.65$ [1]. The low shear configuration of the vacuum magnetic field is, however, modified by internal net plasma currents such as the pressure-driven bootstrap current. The equilibrium currents (Pfirsch-Schlüter currents) generating the Shafranov shift of finite-beta plasmas play an important role and also modify the profile of the rotational transform [2]. Experiments with weak and strong, positive and negative shear were performed by running inductive and EC-driven currents in the appropriate direction.

Although the scenario to operate the same device in net-current-free "stellarator" operation and, for comparison, in pure "tokamak" operation cannot be completely verified on W7-AS (the main coils always impose some external rotational transform), hybrid operation with significant net currents is possible. Configurations with positive and negative shear were investigated and may contribute to the understanding of the physics of reversed-shear tokamak results (e.g., Ref. [3]). Net currents I_p in the range between −30 kA and +30 kA were induced by the ohmic heating (OH) transformer in target plasmas with electron cyclotron resonance heating (ECRH) supplying on-axis deposited heating power of 0.45 MW. The experiments were conducted in long-pulse operation, > 1 s, to obtain steady-state conditions on the current-diffusion time scale. The OH power (typically below 10 kW) can be neglected as compared to the ECRH power. At a feedback-controlled density of typically 2×10^{19} m^{-3} (typical electron and ion temperatures of 3.5 and 0.4 keV, respectively), the electrons dominate the heat transport and ions play a minor role because they are energetically decoupled from the electrons. By a proper choice of the vacuum ι, the discharges were controlled to have an almost constant edge rotational transform of 0.40 ± 0.05. The vacuum ι is 0.55 for −30-kA operation and 0.25 for +30-kA operation, indicating that the plasma current contributes significantly to the total rotational transform. The magnetic configurations for the different net currents deviate significantly from the vacuum configuration, and the corresponding finite-beta stellarator equilibria with net currents were calculated with the NEMEC code. Radial profiles of the electron temperature from Thomson scattering and electron cyclotron emission (ECE) are shown in Fig. 1 (left) for three cases with +30, 0, and −30 kA.

Two distinct effects are clearly seen. First, whereas strong temperature gradients exist within $r/a < 0.3$ for the reference case with zero net current and for all discharges with positive currents, significantly lower central temperatures are measured in the negative current cases. As seen in Fig. 2, a monotonic decrease of T_{e0} with increasing negative current is observed. Second, strong temperature gradients exist in the outer plasma region around $r/a = 0.8$ for all cases with net currents > 5 kA independent of the sign of the current and thus the sign

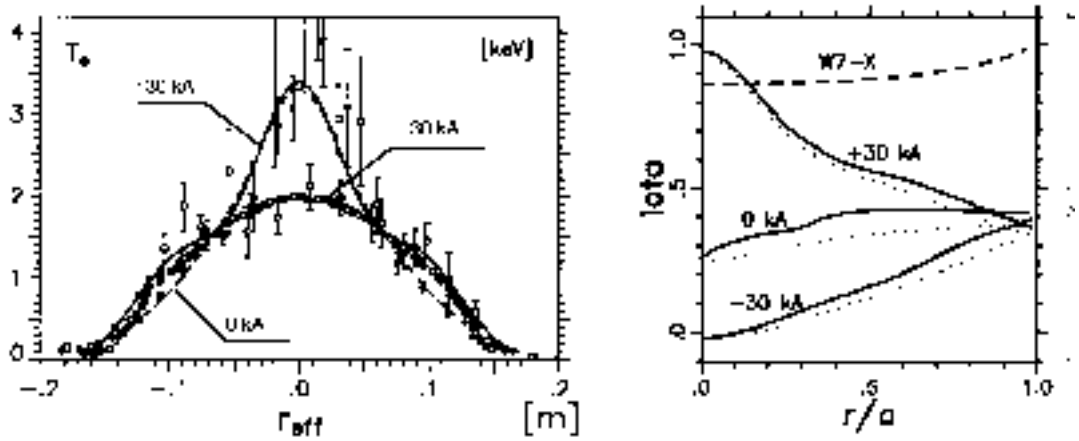

Fig. 1. At left, radial profiles of the electron temperature with currents of −30 kA (dotted line, diamonds), 0 kA (dashed line, dots), and +30 kA (solid line, squares). At right, the corresponding profiles of the total rotational transform (solid lines). The inductive current contribution without bootstrap current is also indicated (dots). The ι profile of W7-X is shown for reference.

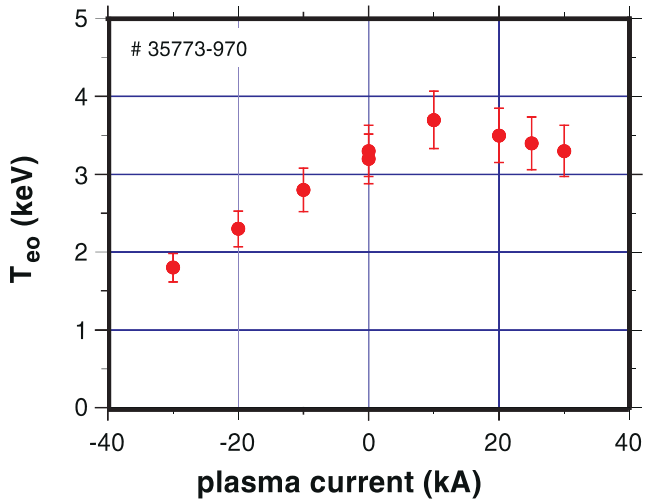

Fig. 2. Central electron temperature for discharges with different plasma currents.

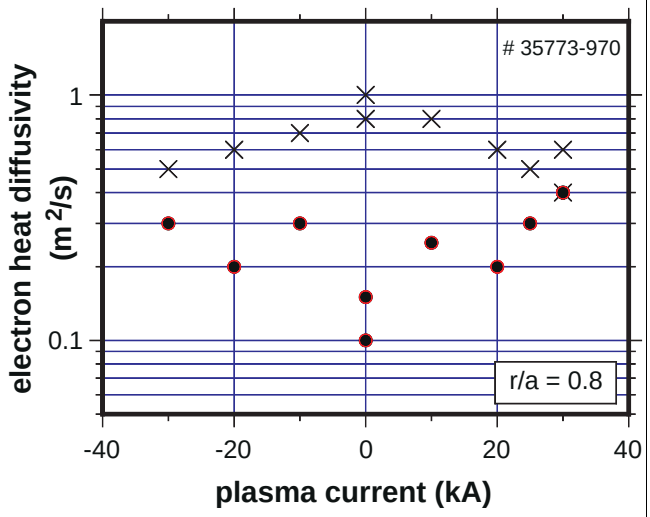

Fig. 3. Comparison of the local electron heat diffusivity (crosses) from power balance analysis with the neoclassical predictions (dots) at r/a = 0.8 for discharges with different plasma currents.

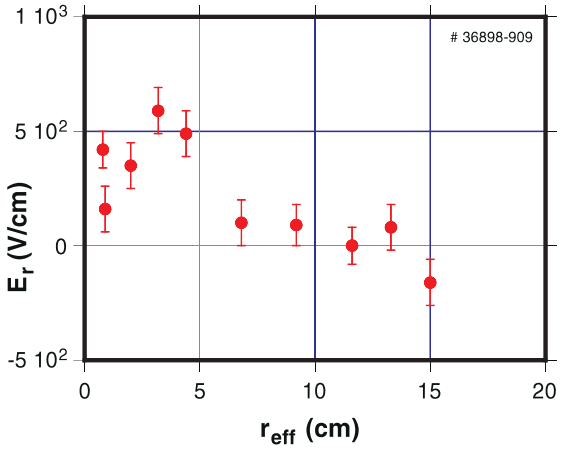

Fig. 5. Radial electric field determined from CXRS as a function of the effective radius in helium discharges.

of the shear. The reference case with zero net current and the same edge ι does not show this steep edge gradient. Net-current-free discharges at optimum confinement at lower $\iota(a) = 0.34$ also show less pronounced gradients, which are in between the two cases of Fig. 1. The ι profiles in Fig. 1 (right) are calculated assuming $Z_{eff} = 2$; the inductive current distribution using the neoclassical resistivity (solid line) and the linear superposition of the bootstrap current contribution (dotted line) are shown. The vacuum ι profile of the W7-X magnetic configuration, which has considerable shear at the edge, is displayed for reference. The current-voltage characteristic gives no evidence for a significant suprathermal electron contribution. Due to the ι-dependence of the bootstrap current (DKES) a self-consistent calculation of the ι profile is necessary. The iteration is robust at positive currents but turns out to be delicate for the negative currents with low or even zero rotational transform in the center.

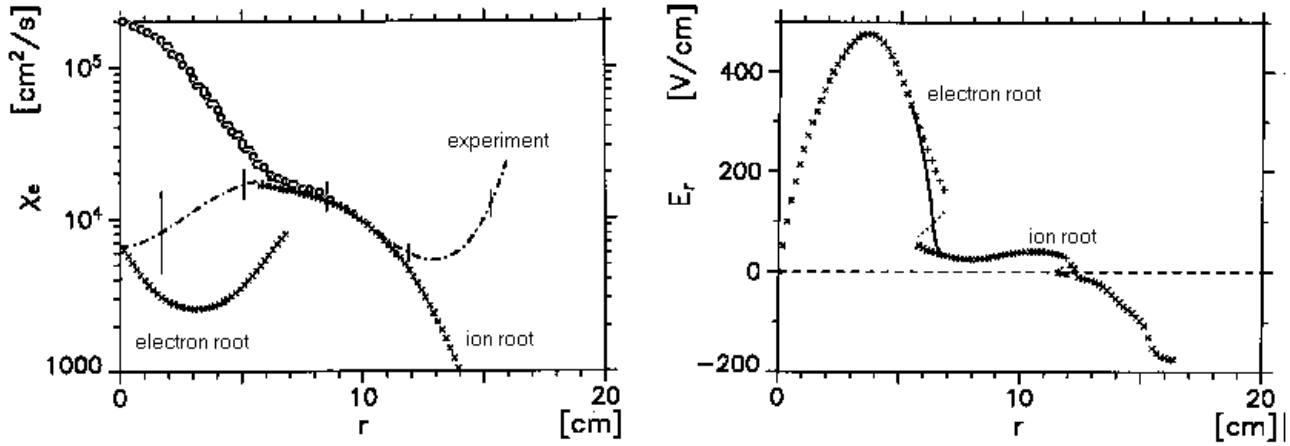

Fig. 4. Electron heat diffusivity (left) and radial ambipolar electric field (right) for the +30-kA case. The neoclassical electron heat diffusivity without (circles) and with (crosses) electric field ("electron root" in the center) is compared to the experimental values (dashed-dotted line).

The ι profiles for negative currents indicate low central values approaching zero in the plasma center, which may explain the central confinement degradation with increasing negative currents. The good confinement in the outer plasma region with both positive and negative net currents may be due to significant shear in this region, which is much smaller in the reference cases with zero net current. The measured local electron heat diffusivity from the steady-state power balance approaches the neoclassical values at high currents even close to the plasma edge up to $r/a < 0.8$, as seen in Fig. 3. This can be interpreted as an expansion of the plasma volume, that is governed by neoclassical transport. Note that neoclassical transport in the long mean free path regime is a strong function of the temperature.

From the neoclassical solution of the ambipolarity condition, the "electron root" for the radial electric field is expected for $r/a < 0.3$. The existence of the electron root and of the related improvement of neoclassical confinement is supported by the heat transport analyses. Assuming the usual approach of zero electric field in the plasma center and of the "ion root" solution, where existing, the neoclassical predictions fit well in the radial range of $0.3 < r/a < 0.8$, but are more than one order of magnitude higher than the measured values in the plasma center with $r/a < 0.3$ (see Fig. 4). The electron root solution with strongly positive radial electric fields must be assumed in the center to reduce the neoclassical transport to below the experimental values.

Direct measurements of the radial electric field were performed with the charge-exchange recombination spectroscopy (CXRS) method in pure helium plasmas. As shown in Fig. 5, the center part of the plasma is governed by positive electric fields of up to 600 V/cm, which supports the theoretical analysis assuming the electron root. Recently central electron temperatures of 4 keV were achieved under these conditions.

J. Baldzuhn, H. Maaßberg, and V. Erckmann for the W7-AS Team
IPP Garching, Garching, Germany
Phone: 0049-89-3299-2129
E-mail: voe@ipp-garching.mpg.de

References

[1] H. Renner, W7-AS Team, NBI Group, ICF Group, and ECRH Group, Plasma Phys. Controlled Fusion **31**, 1579 (1989).

[2] H. Renner, H. Ringler, J. Kisslinger, G. Kühner, W7-AS Team, NBI Group, and ECRH Group, Int. Conf. Plasma Phys. **16C**, Part 1, 501 (1992).

[3] E. J. Strait., L. L. Lau., M.E. Mauel, B. W. Rice, et al., Phys. Rev. Lett. **75**, 4421 (1995).

Potential profiles measured with HIBP and the deduced loss cone structure in CHS

In toroidal helical plasmas, helical-ripple-induced transport and loss-cone loss are greatly affected by radial electric fields. Therefore, measurement of the potential profile is essential to clarify the confinement properties of these plasmas. In CHS, potential profiles in steady-state plasmas have been measured with a 200-keV heavy ion beam probe (HIBP). The potential profiles show widely varying polarity for ECH and NBI plasmas, compared to tokamaks where the potential was observed to be negative. With the HIBP method, singly charged heavy ions (primary beam) are injected into the plasma; some doubly charged ions (secondary beam) emerge from the target plasma with an energy change corresponding to the space potential at their birth point. The analyzer for the HIBP is required to distinguish a few dozen volts of change (potential) in several hundred kilovolt beams (primary beam energy).

In the CHS HIBP, a secondary beam sweep system is introduced in addition to the primary sweep system to manage 3-D trajectories in the toroidal helical plasmas. This method, which we call active trajectory control [1], gives the following advantages: (1) reducing the potential measurement error caused by uncertainty in the angle of the beam injection into the energy analyzer, (2) expanding the applicable configurations and the observation regions, and (3) keeping the energy analyzer away from locations where the magnetic field will disturb the determination of the beam energy.

The experiments presented here were performed on a magnetic field configuration with axis $R_{ax} = 92.1$ cm and a field strength of 0.9 T. The necessary energy is 71 keV for 0.9-T operation when a cesium beam is used. The actual observation points are distributed along the toroidal direction, and the points at left in Fig. 1 are the projections obtained by tracing the magnetic field line from the actual observation points. The toroidal angle ζ_{tor} of the actual observation points is shown at right in Fig. 1, where $\zeta_{tor} = 0$ corresponds to the vertically elongated magnetic flux surface at left in Fig. 1. Other configurations can also be accessed with our system, although the observation region is limited for some configurations.

The upper part of Fig. 2 shows potential profiles obtained during steady-state ECH and NBI plasmas. The open and closed circles indicate the potential profiles of ECH plasmas with low ($n_e = 3 \times 10^{12}$ cm^{-3}) and medium ($n_e = 8 \times 10^{12}$ cm^{-3}) density, respectively. The central electron temperatures of the low- and medium-density cases are $T_e(0) = 900$ eV and $T_e(0) = 400$ eV,

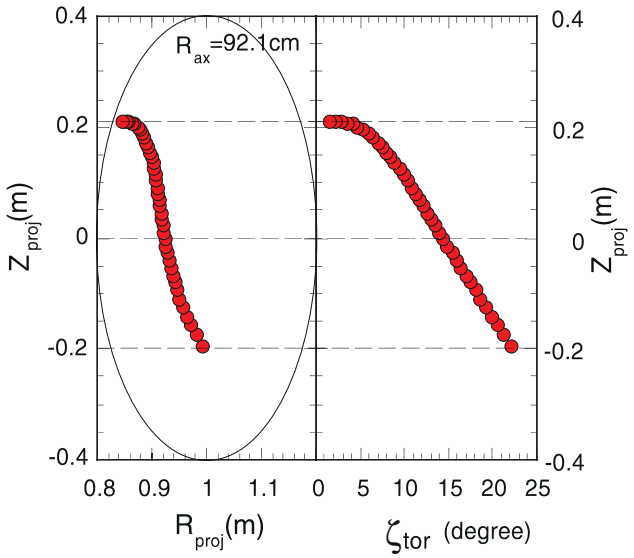

Fig. 1. Left: Projection of observation points with the HIBP.
Right: Toroidal angle of the observation points.

respectively. The squares indicate the potential profile of a co-injected NBI plasma where the electron density is $n_e = 8 \times 10^{12}\,\mathrm{cm}^{-3}$ and the central electron and ion temperatures are $T_e(0) = 300$ eV and $T_i(0) = 200$ eV, respectively. The port-through NBI power was 500 kW. These profiles are averages for about 20 ms in steady state, and the error bars indicate standard deviations.

The potential is positive with a central value of about 200 V for a low-density ECH plasma with gyrotron output power of 100 kW. Electrons are almost in a collisionless regime since the electron collisionality is $\nu_e^*(a/2) = 1.4$. The definition of the collisionality here is $\nu_e^*(r) = \nu_{eff}(r)/\omega_b(r)$ with $\nu_{eff}(r) = \nu(r)/\varepsilon_h$ and $\omega_b = \iota(\varepsilon_h T/m)^{(1/2)}/2\pi R$, where ι is the rotational transform. In the medium-density ECH plasma, the potential exhibits an interesting characteristic; the electric field is positive around the core, while it has a large negative value (= 70 V/cm) near the edge. The electron collisionality is $\nu_e^*(a/2) = 13.1$, and the electrons are in the plateau regime. On the other hand, the potential in the low-density NBI plasma is negative with a central value of about −200 V. The collisionalities of the electrons and ions are $\nu_e^*(a/2) = 6.0$ and $\nu_\iota^*(a/2) = 8.2$, respectively. The electrons and ions are both in the plateau regime.

The lower part of Fig. 2 shows radial electric field profiles deduced from polynomial fitting curves to the obtained potential profiles. In the ECH plasmas, a tendency can be seen — the positive electric field becomes more negative as the density increases. In the medium-density case, the electric field shows a strong shear around the plasma edge, although the statistical error bar is large. In the NBI case, the ion temperature, and

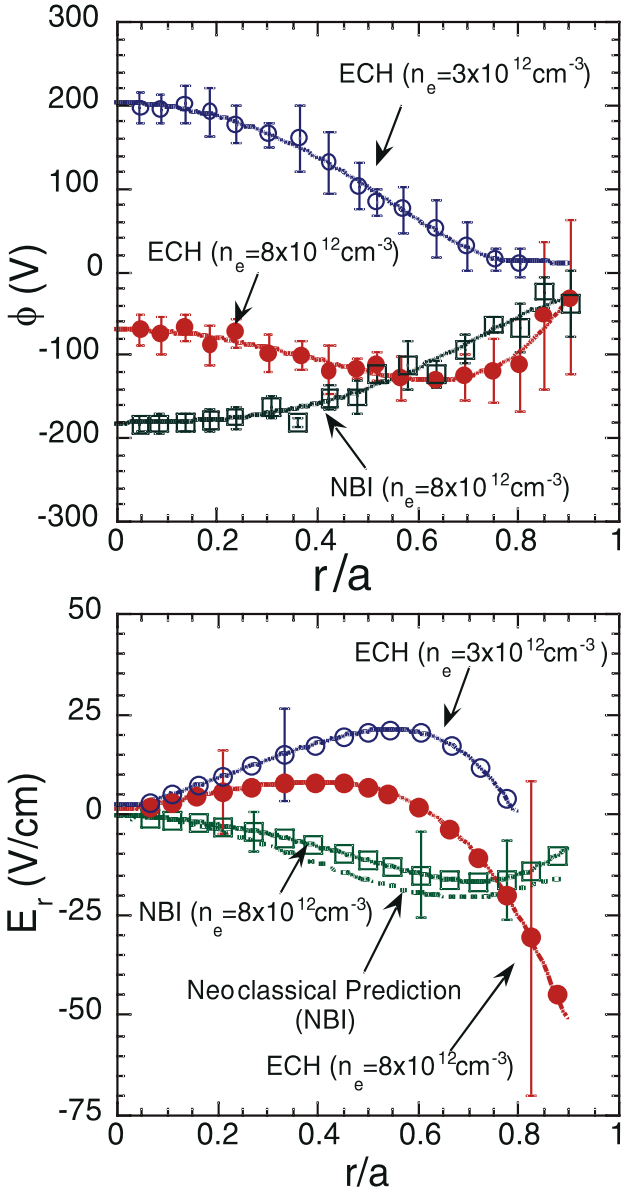

Fig. 2 . Potential profiles (top) and electric field profiles (bottom) in steady state of ECH and NBI plasmas. The electric field profile expected from neoclassical theory is represented by a dotted-dashed line for comparison.

electron density and temperature profiles are available from the database. Hence, the experimentally obtained electric field can be compared with the electric field predicted with the ambipolarity condition $\Gamma_i^{NC}(E_r) = \Gamma_e^{NC}(E_r)$, where $\Gamma_i^{NC}(E_r)$ and $\Gamma_e^{NC}(E_r)$ represent the electron and ion fluxes in the neoclassical theory, respectively. The dashed-dotted line in the lower part of Fig. 2 represents the neoclassical radial electric field for the NBI plasma. The theoretically expected electric field has a tendency similar to that of the experimental result in this case.

These obtained potential profiles give us an insight into loss cone structure and the behavior of high energy

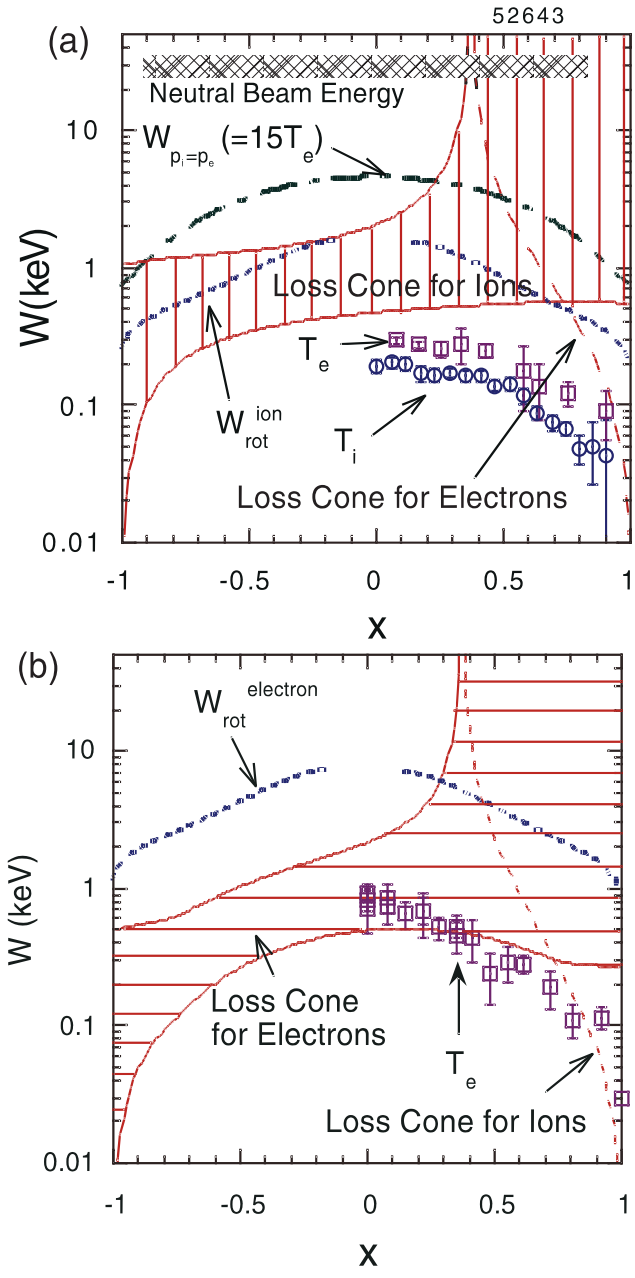

Fig. 3. (a) Loss cone diagrams for deeply trapped ions in NBI plasmas. (b) Loss cone diagrams for deeply trapped electrons in ECH plasmas.

particles. The loss cone structure can be easily estimated from the obtained potential profiles by use of an analytic formula. According to Ref. [2], the loss cone for deeply trapped particles (with small $v_{\|}$) is expressed as $W_m < W < W_p$, where W is the particle energy, $W_m = -q\phi(0) f(x)/[\varepsilon_{ha}(1-x^2)+\varepsilon_{ta}(1-x)]$, and $W_p = -q\phi(0) f(x)/(\varepsilon_{ha}(1-x^2)-\varepsilon_{ta}(1-x))$. Here, ε_{ta} and ε_{ha} represent toroidal and helical ripple coefficients, respectively; x indicates the horizontal coordinate whose origin is on the magnetic axis; and $f(x)$ is a normalized function fitted to the experimental profiles with $f(0) = 1$, $f(1) = f(-1) = 0$. For the magnetic field configuration with $R_{ax} = 92.1$ cm, we choose $\varepsilon_{ta} = 0.16$ and $\varepsilon_{ha} = 0.255$.

The collisionless regime occurs when the helically trapped particles can accomplish one-turn orbits poloidally without a collision. This criterion is roughly expressed as $\omega_{\nabla B} > v/\varepsilon_h$. Figure 3(a) plots the critical energy W_{rot} to satisfy the criterion which is explicitly written as $W_{rot}^{2.5}$ (eV) $> 1.4 \times 10^{-2}\, n_e(\mathrm{cm}^{-3})\, B(\mathrm{T})\, r(\mathrm{cm})^2\, \varepsilon_h^{-2}$. This criterion is no longer valid around the magnetic axis since there the banana width is larger than the local structure owing to the small poloidal field. A loss cone should affect these collisionless particles. Such a loss cone diagram for deeply-trapped particles in the NBI plasma is shown in Fig. 3(a).

When a neutral beam is injected into this plasma, the energy transfer rates to ions and electrons are a function of the electron temperature. The beam energy at which energy is transferred equally to ions and electrons is $W_{Pi=Pe} = 15 T_e A_b [Z_i^2/A_i]^{2/3}$, where A_b, A_i, and Z_i are the atomic mass of the beam particles, and the atomic mass and the charge of the bulk plasmas, respectively. Above this energy ($15\ T_e$), the beam particles selectively heat electrons, preserving their pitch angle. On the other hand, the injected beam particles experience pitch-angle scattering in the region below this energy and simultaneously transfer their energy to ions. The beam particles are therefore more likely to enter the loss cone below this energy.

The neutral beam is tangentially injected in the CHS with an energy of about 38 keV [the hatched region in Fig. 3(a)]. Effective energy transfer from injected beam to bulk ions occurs in the regime between the upper loss cone boundary and $W_{Pi=Pe}$ ($= 15T_e$). For the bulk ions, their temperature is below the lower loss cone boundary. Hence, the bulk ions are confined by the rotation due to **E×B** motion. If the potential becomes sufficiently negative for the loss cone region to be located above $W_{pi=Pe}$ line, fast ions pass through the region because they have mostly parallel velocity, i.e., the loss cone region in the figure is not a real loss cone for beam ions. Therefore, the ion heating efficiency will be improved since the pitch-angle scattering will occur below the loss cone

region. The dashed line in Fig. 3(a) shows the loss cone for electrons in the NBI plasma.

A loss cone diagram for deeply trapped electrons can be also demonstrated for the low-density ECH plasma with a positive potential shown in Fig. 3(b). Here that the loss cone region above W_{rot} exists only on the outside ($x > 0$). The critical energy W_{rot} for electrons is higher than that for ions since the collision frequency is larger for the same energy; $W_{rot}^{2.5}$ (eV) $> 6.3 \times 10^{-1}\, n_e$ (cm^{-3}) B (T) r (cm)$^2\, \varepsilon_h^{-2}$. Thus, an electron heated up by the wave on the outside of torus will easily enter the loss cone. For the ions, the loss cone region in this positive potential is localized only in an outside periphery of the plasma as is shown by the dashed line in Fig. 3(b). Therefore, highly effective heating due to high-energy ions is expected while positive potential is maintained for the plasma because no $\mathbf{E} \times \mathbf{B}$ resonance exists for the ions.

A. Fujisawa for the CHS group
National Institute for Fusion Science
Nagoya 464-01, Japan
Phone: 052-789-4246
Fax: 052-789-4203

References

[1] A. Fujisawa et al., Rev. Sci. Instrum. **63,** 3694 (1992).

[2] K. Itoh et al., Phys. Fluids B **3,** 1294 (1991).

Omnigenous stellarators

Stellarators are attractive plasma confinement devices. With externally generated rotational transform, they can be run in steady state without complicated current drive schemes, and stellarators are not susceptible to disrup - tions. Unfortunately, the original stellarator designs had large particle loss rates because they contained particles (those locally trapped in a helical magnetic well) with large drift orbits that intersected the wall. This has led to a search (e.g., Ref. [1]) for configurations lacking such particles. Here we point out that good confinement can be attained with restrictions less restrictive than previ - ously thought.

Nearly a decade ago, Nührenberg and Zille [2] proposed that stellarators be quasihelical (termed quasisymmetric in recent work [3]), meaning that the magnetic strength B is a function of only a single linear combination of the toroidal and poloidal angles in Boozer [4] coordinates. They were able to find large-aspect-ratio quasihelical systems. However, Garren and Boozer [5] found that the condition of quasihelicity cannot be satisfied beyond a certain order in an expansion in the distance from the magnetic axis. This result led to a pessimistic view about the existence of small-aspect-ratio stellarators with good transport properties.

We have recently shown [6] that omnigenous systems [7], those for which the bounce-averaged drift remains within a flux surface, form a larger class than quasiheli - cal systems. (The details of our discussion appear in Ref. [8].) We have obtained a precise condition for omnige - neity: the contours of magnetic strength B on a magnetic surface must have constant angular separation in Boozer coordinates. We also show that omnigenous systems for which the magnetic strength is an analytic function must be quasihelical, yet one can have systems with analytic magnetic strength functions that are far from quasihelical while very nearly omnigenous. This last result indicates that, in a practical sense, analytic near- omnigenous sys- tems form a larger class than quasihelical systems. Finally, we propose simple design criteria for systems with good confinement properties.

Our results are related to those of Ref. [3], where it was noted that isometric systems, those for which the mag - netic contours within a surface are separated by constant distance along a magnetic field line, are omnigenous. Our condition of constant angular separation is equiva - lent to isometry. Our results are most easily arrived at from the use of Littlejohn's Lagrangian [9] in Boozer coordinates. Boozer coordinates are flux coordinates, implying that the magnetic field has a trivial, periodic- angle Clebsch representation,

$\boldsymbol{B} = \nabla\psi \times \nabla\theta + \iota(\psi)\nabla\varphi \times \nabla\theta$. This implies that the vector potential has the form $\boldsymbol{A} = \psi\nabla\theta + A_\varphi(\psi)\nabla\varphi$, where $\iota = -\mathrm{d}A_\varphi/\mathrm{d}\psi$. As noted by Boozer, these angles can be further specified by requiring that the magnetic field, $\boldsymbol{B} = B_\psi(\psi,\theta,\varphi)\nabla\psi + B_\theta(\psi)\nabla\theta + B_\varphi(\psi)\nabla\varphi$, have angular covariant components that are flux functions.

Quasihelical systems are those for which B is a function of only a single linear combination of the angles, say $\zeta \equiv N\varphi - l\theta$, where N is the toroidal mode number and l is the poloidal mode number of the dominant Fourier component of the magnetic field strength. [Near-axis analysis [6] shows that $l = 1$.] For such systems, it follows directly from the Littlejohn Lagrangian that

$$P_\mathrm{h} \triangleq \frac{\partial L_{gc}}{\partial \dot{\theta}} = \frac{e}{c}\left(\psi + \frac{A_\varphi}{N}\right) + \frac{mu}{B}\left(B_\theta + \frac{B_\varphi}{N}\right),$$

the helical canonical guiding-center momentum, is an invariant of the motion. Analogous to the axisymmetric case, the existence of the invariant P_h guarantees orbits with good properties. Energy conservation guarantees that the variation of the parallel velocity u and, hence, the final term is bounded. Thus, the variation of $\psi + \frac{A_\varphi}{N}$ is small, so orbits remain confined to the vicinity of a flux surface.

A less restrictive way to achieve systems with good trajectories is to require omnigeneity [7], the property whereby the bounce-averaged cross-flux-surface drift vanishes. As the bounce-averaged drift conserves the bounce (or longitudinal) action through lowest order in the expansion in the drift frequency relative to the bounce frequency, this implies that the bounce action is constant on a surface. Thus, we need to find systems where the bounce action, or zeroth-order bounce adiabatic invariant,

$$J_0 = \oint mu\hat{\boldsymbol{b}} \cdot \mathrm{d}\boldsymbol{r} = m\left(\iota B_\theta + B_\varphi\right) \oint \left(u\,\mathrm{d}\varphi/B\right) \quad ,$$

is constant on a magnetic surface. Here the velocity $u = [2(E - \mu B - e\Phi/m)]^{1/2}$ is determined by energy conservation, and the loop integral is along a field line between reflection points, $E = \mu B$. An immediate consequence of the condition that J_0 is constant on a magnetic surface is that the local minima of the magnetic field along field lines in a given surface have the same value of B. This is the principle behind the improved confinement for the systems in Ref. [1]. One can also show that the magnetic maxima and the action of particles at the trapped-passing boundary have the same value on a surface and, hence, that transition orbits [10], which are chaotic owing to separatrix crossing [11], are absent in omnigenous systems. We are able to show from the form of the bounce action in Boozer coordinates that the angular separation along a magnetic field line of any two contours of the same value of B is constant on a magnetic surface. From this follow many consequences. First, it can be shown that the contour of the maxima is straight in Boozer coordinates provided the rotational transform is irrational. Second, one can construct omnigenous functions B that depend nontrivially on θ in addition to ζ. Unfortunately, this construction leads to nonanalytic transformations unless the transformation is independent of θ. Thus, analytic, omnigenous magnetic fields are quasihelical.

However, analyticity is a fragile concept. Two functions, one analytic and one not, can be arbitrarily close in value everywhere. Hence, it might be possible to find a magnetic strength that is analytic, yet is close everywhere to a nonanalytic function that is far from quasihelical. If this is true, then it is possible to have magnetic fields that are very far from quasihelical, yet very nearly omnigenous.

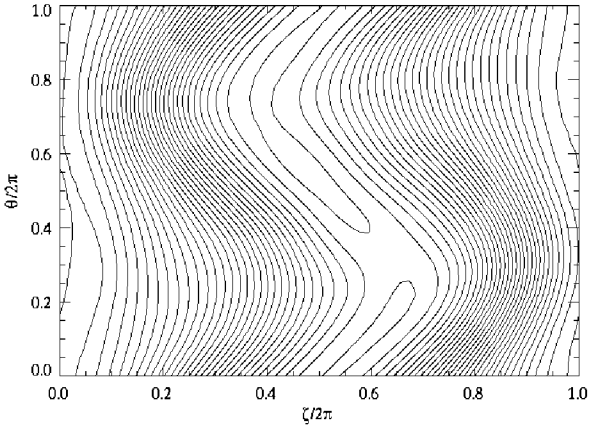

Fig. 1. Contours of an near-omnigenous, analytic $|\boldsymbol{B}|$ that is far from quasihelical.

To test this idea, we used our method to construct a nonanalytic, omnigenous $|\boldsymbol{B}|$ that is far from quasihelical. The contours of this magnetic field strength are shown in Fig. 1. That this field is not quasihelical is evidenced by the fact that the contours are not straight lines. However, the contours of $|\boldsymbol{B}|$ have nearly constant separation along a field line, as required for omnigenity. To test the omnigeneity of these configurations, we integrated several trajectories in the analytic, nearly omnigenous magnetic field found above. The poloidal cross section of the trajectory of a typical locally trapped particle is shown in Fig. 2. [The coordinates are $x = r\cos\theta$ and $y = r\sin\theta$, where $r = [\psi/\psi_\mathrm{edge}]^{1/2}$, and B_0 is the value of the magnetic field on axis]. We have taken a relative ripple at the edge of 25%. We set the dimensionless energy, $E/m\Omega_0^2a^2 = 2 \times 10^{-3}$, and the magnetic moment, $\mu B_0/m\Omega_0^2a^2 = 1.81 \times 10^{-3}$, where E is the energy, Ω_0 is the gyrofrequency on axis, and a is the minor radius. This corresponds to a 17-keV proton in a machine with a 1-T magnetic field and a minor radius of 30 cm. This figure shows that the trajectory has remained, on

average, close to its initial flux surface. One can see that this system is not quasihelical by the fact that the oscilla - tion width varies with poloidal angle.

Ultimately one would like to set certain limited criteria for the design of a stellarator, as one does not expect to obtain perfectly omnigenous systems. The condition proposed in Ref. [1] is that of constant magnetic minima, so that the deeply trapped particles are omnigenous. As noted above, the conditions of constant magnetic maxima and constant separatrix action of a surface ensure both omnigeneity of the marginally trapped parti - cles and elimination of the chaotic transition particles. With all three conditions, the two extremes of locally trapped particles are omnigenous, and there are no cha - otic trajectories. We suggest these as starting design cri - teria, though naturally it will be necessary to check such systems to ensure that the trajectories of the intermedi - ately trapped particles do not make excessive drift excur - sions. In addition, these systems should have better con - finement than toroidal systems with equal magnetic field variation; the variation of the flux surface label along a trajectory is smaller than that in a tokamak by the ratio, $N/\iota - 1$, of connection lengths. Indeed, this leads to the interesting speculation that transport due to ballooning mode turbulence, which increases with connection length, will also be small in omnigenous helical systems.

This work was supported by the U. S. Department of Energy under grant DE-FG003-95ER54297.

John R. Cary and Svetlana G. Shasharina
Center for Integrated Plasma Studies and Department of Physics
University of Colorado
Boulder, CO 80309-0390
E-mail: cary@boulder.colorado.edu

References

[1] H. E. Mynick, T. K. Chu, and A. H. Boozer, Phys. Rev. Lett. **48**, 322 (1982).

[2] J. Nührenberg and R. Zille, Phys. Lett. A **129**, 113 (1988).

[3] A. A. Skovoroda and V. D. Shafranov, Plasma Phys. Rep. **21**, 937 (1995).

[4] A. H. Boozer, Phys. Fluids **24**, 1999 (1981).

[5] D. A. Garren and A. H. Boozer, Phys. Fluids B **3**, 2822 (1991).

[6] J. R. Cary and S. G. Shasharina, Phys. Rev. Lett. (1997).

[7] L. S. Hall and B. McNamara, Phys. Fluids **18**, 552 (1975).

[8] J. R. Cary and S. G. Shasharina, in preparation (1996).

[9] R. G. Littlejohn, J. Plasma Phys. **29**, 111 (1983).

[10] J. R. Cary, C. L. Hedrick, and J. S. Tolliver, Phys. Fluids **31**, 1586 (1988).

[11] C. R. Menyuk, Phys. Rev. A **31**, 3282 (1985); J. R. Cary, D. F. Escande, and J. L. Tennyson, Phys. Rev. A **32**, 4256 (1986); A. I. Neishtadt, Sov. J. Plasma Phys. **12**, 568 (1986); J. R. Cary and R. T. Skodje, Physica D **36**, 287 (1989).

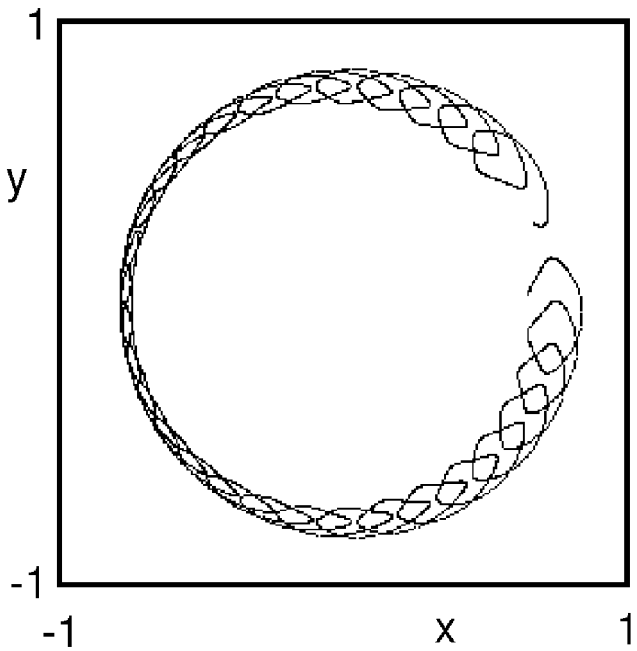

Fig. 2. Poloidal cross section of a typical locally trapped particle in the nearly omnigenous magnetic field.

Four-period quasihelically-symmetric Heliac

The quasihelically symmetric stellarator (QHS) discov- ered by J. Nührenberg and R. Zille [1] possesses the advantage of low neoclassical transport which can be on the level of tokamak losses. Quasisymmetric stellarators are studied both with three-dimensional (3-D) codes and with the paraxial approximation. The existence of differ - ent types of quasisymmetry [2] makes the problem of comparing their equilibrium, stability, transport, and other properties relevant.

The paraxial approximation shows that in Heliac-like QHS systems, in which the magnetic surface cross sec - tion rotates in phase with the principal normal to the magnetic axis, the fulfillment of the quasisymmetry con - dition can be combined with a large magnetic well. For Helias-like QHS systems, in which the magnetic surface cross section lags behind the principal normal with respect to the position of the magnetic axis by half a turn in one period, the exact fulfillment of the QHS condition decreases the magnetic well.

The accuracy of the quasisymmetry condition in differ - ent systems — Heliac-like and Helias-like — can be characterized by the ratio X of the dominant quasihelical symmetric Fourier component (1,1) of the magnetic field strength in Boozer coordinates to the maximum Fourier component that violates the symmetry, evaluated at the plasma boundary.

The first 3-D calculations [1] of QHS systems showed that the optimization of a Helias towards quasisymmetry (X is more than 10 and high fulfillment of the QHS condition) leads to configurations without a magnetic well. A magnetic well could be achieved only with low X. In a 6-period Helias, the stability limit occurs at β = 5%, where $\beta = 2\langle p \rangle / B_0^2$, with B_0 the magnetic field strength on the magnetic axis, and p the plasma pressure with an assumed parabolic profile. Later the optimization of a 5-period Helias proposed for W-7X, with stability up to β = 5%, sacrificed quasisymmetry to reduce the bootstrap current and the parallel current density. Still, relatively good particle confinement and reduced neoclassical losses are guaranteed through poloidally closed contours of the second adiabatic invariant, J.

A new project, the Helically Symmetric eXperiment (HSX) at the University of Wisconsin, Madison, USA [3], is a 4-period QHS Helias with X = 5–7 that is stable with respect to Mercier modes up to β = 0.8% and β = 1.66% for the standard and deep well configurations.

Heliac-like stellarators without quasisymmetry ($X \sim 1$) can have a large magnetic well. The 4-period HHH Heliac-like stellarator can achieve Mercier stability up to β = 7.3% on the outer half of the plasma radius [4]. In the conventional 4-period heliac TJ-II [5], one can obtain Mercier stability up to β = 5%, if the island problem is not taken into account.

We have investigated the local ideal MHD stability properties of a 4-period quasisymmetric Heliac-like stellarator, shown in Fig. 1. This type of quasisymmetry can provide more possibilities of obtaining a magnetic well.

Paraxial estimates show that the β -limit from equilibrium and Mercier stability can be achieved at the level of 8% for an initial magnetic surface cross-section elongation E_0 = 5.5 and that β =5% can be achieved for E_0 = 3. The fulfillment of the quasisymmetry condition in the paraxial approximation makes the shape of the magnetic surface for Heliac-like systems very complicated.

To validate the paraxial estimates, we need to obtain the Fourier spectrum for 3-D equilibrium and stability codes. For aspect ratio A = 10 and initial elongation E_0 = 3, the Fourier spectrum of the quasisymmetric Heliac boundary in cylindrical coordinates has a large number of components. So we need to modify our spectrum to get 3-D quasisymmetry. The VMEC input boundary of a 4-period Heliac with 2 poloidal and 4 toroidal modes achieves a relatively weak quasisymmetry condition (X = 3).

Calculations of 3-D equilibria with the VMEC code yield a beta limit of β = 9.8% for a parabolic pressure profile. The stability of a 4-period Heliac-like stellarator has also been investigated with the TERPSICHORE code. The Mercier criterion is positive (stable) up to β = 4%. Thus, the 3-D calculations of Mercier stability in our configuration with E_0 = 3 give a lower beta-limit than the paraxial estimates. The Mercier criterion imposes a less restrictive limit than the ballooning modes, for which β = 1.4%.

The ballooning stability in quasisymmetric Heliac-like systems and also the influence of the accuracy of quasi-symmetric conditions on particle orbits and transport need further investigation.

M. Yu. Isaev, W. A. Cooper,† S. Yu. Medvedev,‡ M. I. Mikhailov, V. D. Shafranov, A. A. Subbotin
Nuclear Fusion Institute, Russian Research Centre
Kurchatov Institute, 123182, Moscow, Russia
† Centre de Recherches en Physique de Plasmas
Association Euratom - Confédération Suisse,
Ecole Polytechnique Fédérale de Lausanne, Switzerland.
‡ Keldysh Insitute of Applied Mathematics,
Russian Academy of Sciences, Moscow, Russia.
E-mail: ISAEV@qq.nfi.kiae.su

References

[1] J. Nührenberg and R. Zille, Phys. Lett. A **129**, 133 (1988).

[2] M. Yu. Isaev, M. I. Mikhailov, and V. D. Shafranov, Plasma Phys. Rep. **20**, 319 (1994).

[3] P. G. Matthews et al.,. Proc. of 10th Int. Conf. on Stellarators, Madrid, 1995 (IEAE, Vienna, 1995). p. 167.

[4] M. Yokoyama, Y. Nakamura, and M. Wakatani, Trans. Fusion Technol. (Proc. 6 Int. Toki Conf., Japan, 1994) **27**, 186 (1995).

[5] C. Alejaldre et al., Fusion Technol. **17**, 131 (1990).

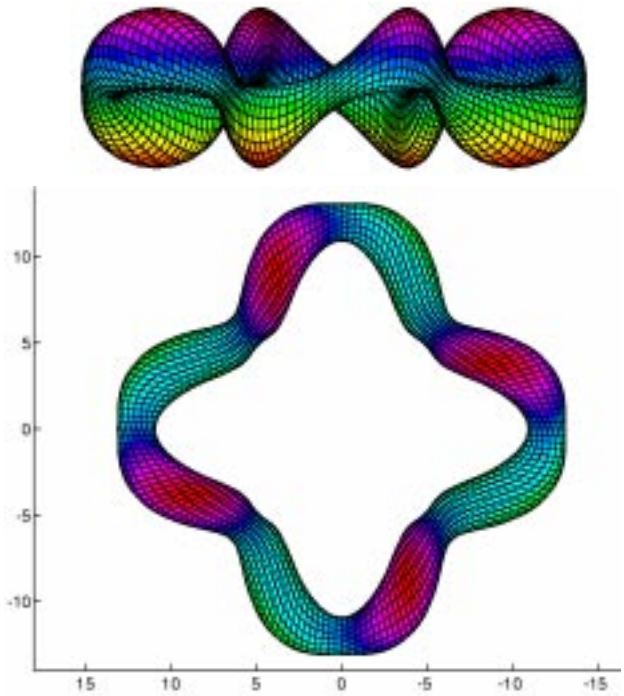

Fig. 1. The quasisymmetric Helias.